Phospholipid—Gold Nanorod Composites

Christopher J. Orendorff,* Todd M. Alam, Darryl Y. Sasaki, Bruce C. Bunker, and James A. Voigt

Sandia National Laboratories, Albuquerque, New Mexico 87185

ABSTRACT Phospholipids comprise an enormous range of chemical structures that provide much of the functionality associated with cellular membranes. We have developed a simple method for incorporating phospholipids onto the surfaces of anisotropic gold nanorods as a stepping-stone for creating responsive and multifunctional nanocomposites. In this report, we demonstrate how phospholipids can be used to control the self-assembly of gold nanorods into agglomerate architectures ranging from open "end-to-end" networks to densely packed "side-to-side" arrays. The results indicate that lipid—gold nanorod assembly is governed by the tuning of electrostatic interactions within the phospholipid layers as well as by how the phospholipid layers organize themselves around anisotropic nanorod surfaces.

KEYWORDS: gold nanorods · lipid bilayer · surface modification · self-assembly · nanocomposites

Noble metal nanorods and nanowires are known to exhibit unique optoelectronic, mechanical, electronic, and chemical properties due to their anisotropy and tunability of size and shape.[1] Gold nanorods are of particular interest due to their stability under ambient conditions relative to other metals, such as silver and copper. Static assemblies of gold nanorods and gold nanorod composite materials into 1D, 2D, and 3D structures have been generated by a variety of techniques. For example, linear 1D assemblies of gold nanorods have been shown using biologically[2,3] and chemically directed approaches.[4] There are numerous reports of liquid crystalline assemblies of metal nanorods in two or three dimensions using chemically directed approaches,[5−8] biodirecting methods,[9] Langmuir−Blodgett techniques,[10,11] and ionic strength induced flocculation.[12−14]

Our primary interest is in using gold nanorods in composite materials, where the assembly of nanorods is switchable, reconfigurable, and dynamic. Most examples of gold nanorod assembly in the literature are for static assemblies, where there is no switchability or reversibility in the process. However, there are examples in the literature of metal nanoparticle assemblies that are switchable. For example, by using a crown-ether-like ligand, Obare *et al.* have shown the controlled assembly of gold nanoparticles as a function of aqueous lithium ion concentration.[15] In addition, gold nanorods have been switched between a random assembly to a 2D liquid crystalline assembly using a pH-triggered diacid bridging molecule.[16] While both of these are examples of more dynamic assemblies, their resultant structures are essentially irreversible from a practical perspective because the reverse step involves increasing the solution ionic strength which would precipitate out the nanocomposite of interest.

In considering functionally dynamic coatings for gold nanorods, lipid bilayers offer a biocompatible interface that can display a broad range of reactive and interactive functionality existing in specific structural phases.[17] Additionally, synthetic lipid membranes have been used as simple models of the cell membrane enabling the incorporation and functional properties of membrane-associated proteins.[18] Most relevant to the current work is the facile formation of supported lipid bilayers onto solid surfaces.[19] The supported bilayer readily interfaces with hydrophilic surfaces, such as glass, mica, and silicon, to generate a conformal and virtually defect-free coating. Coupling to metal surfaces has also been achieved but typically through tethered approaches that chemically link the bilayer to the surface, such as through a gold−thiolate bond. Phospholipid vesicles are known to adsorb intact to gold surfaces but, due to a lack of membrane−surface attraction, resist rupturing to form the supported bilayer.[20] Recent work, however, has found that supported bilayers can be

*Address correspondence to corendo@sandia.gov.

Received for review January 14, 2009 and accepted March 09, 2009.

Published online March 24, 2009.
10.1021/nn900037k CCC: $40.75

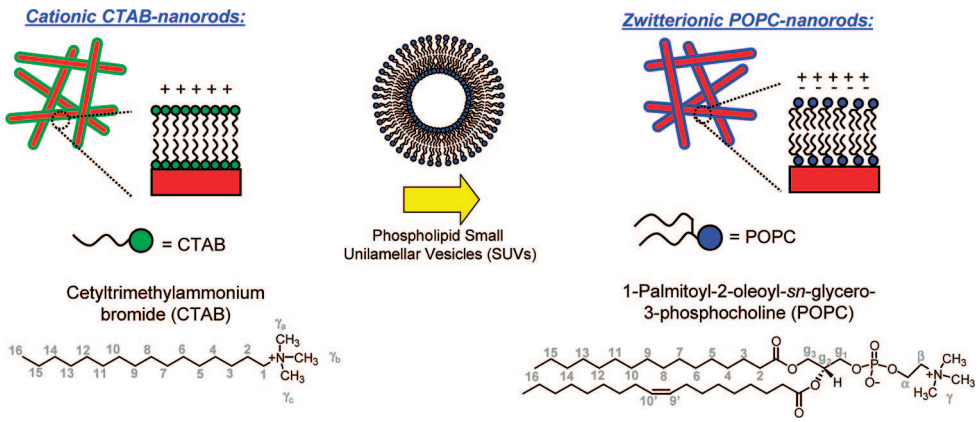

Figure 1. Cartoon of the modification process of as-prepared CTAB−gold nanorods with phospholipid liposomes.

formed on gold by inducing vesicle rupturing with viral peptides.[21] Moreover, modification of gold nanorods by phospholipids has been reported as a means of reducing the cytotoxicity of metal nanoparticles.[22]

We have developed a strategy for the assembly of nanocomposite materials based on lipid-protected gold nanorods. Using a vesicle fusion approach, we modified the initial cetyltrimethylammonium bromide (CTAB) surfactant coating on the nanorods with a lipid bilayer and demonstrate its formation spectroscopically. In this report, we describe the synthesis and tunable properties of lipid-protected gold nanorods. We also present the self-assembly and controlled disassembly of these composites in an effort to move toward reversible reconfigurable nanomaterials. These initial studies on passive lipid-functionalized nanorods could serve as the groundwork for introducing active components into these systems to make switchable or reconfigurable nanocomposite materials.

RESULTS

CTAB−Gold Nanorods. Gold nanorods were prepared by the seed-mediated, surfactant-directed approach described by Murphy *et al.*[23,24] As-prepared gold nanorods are capped with a bilayer of CTAB, giving these nanorods a net positive surface charge (approximately +40 mV) from the quaternary ammonium surfactant headgroup.[25] While the nature of the CTAB−gold interaction is the subject of some debate, there is evidence to suggest it is mediated by electrostatic interactions between adsorbed bromide anions at the gold nanorod surface.[1,25] In addition, the surfactant bilayer is stabilized by hydrophobic interchain coupling interactions within the bilayer.[26] There has been significant interest in modifying the surface of these nanorods to give them specific functionality. While alkanethiols[2,27] and polymers[28] have been used to modify the surfaces of gold nanorods, evidence to support the displacement of CTAB capping molecules with a different surface capping agent has been limited.

Lipid−Gold Nanorod Composites. The approach described in this report is to modify the surface of gold nanorods with phospholipid vesicles by exchange or displacement of CTAB at the nanorod surface. Although phosphotidylcholine lipids differ from CTAB surfactant in net electrostatic charge at neutral pH, both are terminated with trimethylammonium headgroups that may interact similarly with the gold nanorod surface. Phospholipid−gold nanorod composites were prepared by modification of the gold nanorod surface with POPC liposomes. Figure 1 shows a cartoon of the modification process. Excess CTAB surfactant was removed from the CTAB−gold nanorod sample such that the final CTAB concentration is estimated to be 40 μM in 1 mL (2×10^{11} particles, determined by the absorption spectrum, the average nanorod size, and the assumption of a bilayer of CTAB).[29] The gold nanorod surface was modified with phospholipids by dispersing CTAB−gold nanorods in 2 mL aqueous solutions containing a 10 mM POPC liposome (~1000-fold molar excess relative to the estimated CTAB concentration). After an adsorption time of 12 h, POPC−gold nanorods are centrifuged twice and redispersed in water to remove displaced CTAB and unbound POPC.

The exchange of the CTAB capping layer on the gold nanorods by POPC was monitored by ^{1}H NMR, as well as by FT-IR spectroscopy. Figure 2a−d shows the ^{1}H NMR spectra for CTAB (10 mM), POPC (10 mM), CTAB−gold nanorod (40 μM), and POPC−gold nanorod (20 μM) samples. All nanorod samples were centrifuged and redispersed in D_2O prior to NMR spectral acquisition in order to remove excess or unbound surfactant and lipid. Table 1 summarizes the ^{1}H chemical shifts for these different samples. The chemical shift assignments have been previously reported.[30−33] For the CTAB−gold nanorod composites, a slight decrease in the chemical shift was observed in comparison to free CTAB. This is particularly true for the γ-methyl protons and the 1- and 2-methylene protons near the headgroup (see Figure 1 for the numbering of the different protons in CTAB and POPC). These results support the picture of CTAB binding to the gold nanorod surface through the trimethylammonium headgroup. This shift of −0.05 to −0.04 ppm for the headgroup protons is similar to that observed for CTAB-coated Au nanospheres, as well as the −0.07 ppm shift reported for CTAB-capped Au nanorods.[30] Similar decreases in the ^{1}H NMR chemical shifts of protons near the headgroup have also been observed for CTAB-capped gold

TABLE 1. ^{1}H NMR Chemical Shifts, Line Widths, and Assignments for CTAB, POPC, and Nanorod Composites

^{1}H ppm (fwhm Hz)[a]		
CTAB	CTAB/nanorods	assignment[b]
0.89−0.91 (8, 7.5)	0.88 (27)	16 (CH_3)
1.33 (71)	1.30 (70)	4−15 (CH_2)
1.41 (13)	1.38 (26)	3 (CH_2)
1.82 (19)	1.78 (29)	2 (CH_2)
3.16 (10))	3.11 (25)	γ (CH_3)
3.37 (23)	3.31 (20)	1 (CH_2)
^{1}H ppm (fwhm Hz)[a]		
POPC	POPC/nanorods	assignment[c]
0.90 (22)	0.90 (46)	16 (CH_3)
1.30 (64)	1.30 (480 [71%], 57 [29%])[d]	4−15, 4′−7′, 12′−17′ (CH_2)
1.62 (95)	1.61 (100)	3,3′ (CH_2)
2.05 (45)	2.03 (40)	8′,11′ (CH_2)
2.36,2.41 (85,43)	2.37 (100)	2,2′ (CH_2)
3.27 (10)	3.26 (167 [74%], 20 [26%])[d]	γ(CH_3
3.70 (18)	3.70 (33)	α (CH_2)
4.02 (77)	*e*	g_1 (CH_2)
4.24 (35)	*e*	g_3 (CH_2)
4.31 (24)	4.31 (48)	β (CH_2)
4.45 (32)	*e*	$g_{1'}$ (CH_2)
5.3 (29)	*e*	g_2 (CH)
5.35 (64)	5.31 (65)	9′,10′ (CH)

[a]Full width at half-maximum (fwhm) line width. NMR spectra were obtained at 298 K for CTAB and CTAB/nanorod samples and at 315 K for POPC and POPC/nanorod samples. [b]Assignments based on previous CTAB results from refs 30 and 31. [c]Assignment based on previous egg-PC and POPC literature from refs 32 and 33. [d]Deconvolution of a broad and narrow component including relative percent in square brackets. [e]Resonances not observed or unresolved due to increased line broadening.

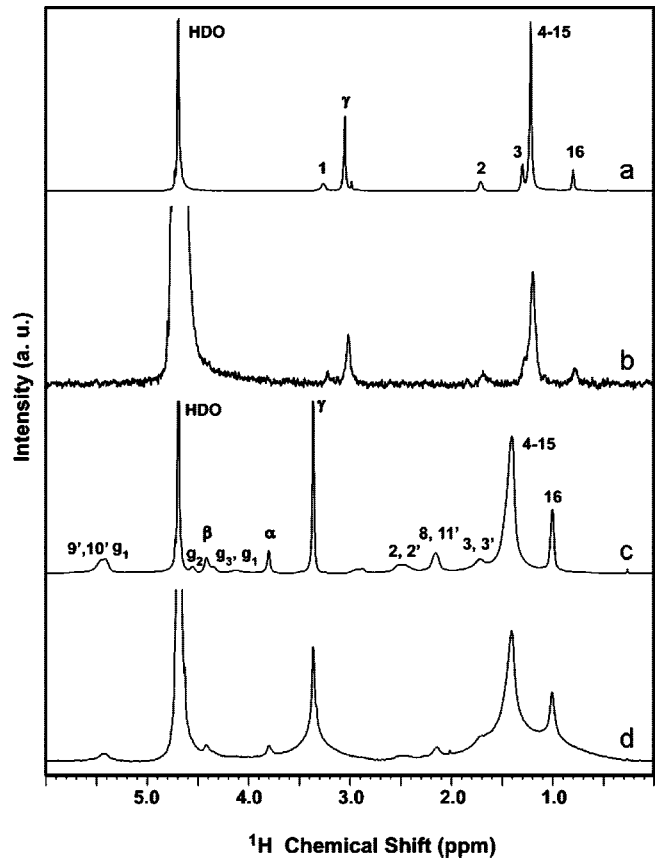

Figure 2. ^{1}H NMR spectra of (a) 10 mM CTAB, (b) CTAB-protected gold nanorods, (c) 10 mM POPC SUVs, and (d) POPC-protected gold nanorods. All spectra were acquired in D_2O.

nanoparticles.[34] These chemical shift variations have been attributed to a Knight shift due to the close spatial contact between headgroup protons and the Au surface. The increase in the full width at half-maximum (fwhm) line width for the γ-, 2-, and 3-headgroup protons of CTAB (Table 1) is also consistent with a reduced mobility resulting from the interaction of CTAB with the Au nanorod. It should be noted that the chemical shift and line width variation in CTAB−gold nanorods were significantly smaller than the dramatic line width variations observed in the ^{13}C NMR of alkanethiol monolayers on gold[35] or the significant chemical shift changes in the ^{1}H NMR of alkylamines and aminoalcohols interacting with Au nanoparticles.[36−38] The smaller variation of chemical shift and line width most likely reflects the weaker coordination and ionic interaction of CTAB to the gold surface in comparison to the thiol and amine binding on gold nanoparticles. It has been suggested that the ^{1}H NMR spectrum of the CTAB-capped gold nanorods in Figure 2 may only reflect headgroup environments that are in outer leaflet of the proposed bilayer structure, and that the headgroup protons that are directly adsorbed to the gold surface are broadened beyond detection. Integration of the γ-methyl and the C_{16}-methyl signal demonstrates that all the protons of the entire CTAB molecule were observed, and that this selective loss of protons near the surface from the NMR spectrum is not occurring. If one assumes a bilayer structure, the observation of a single set of resonances (especially for the headgroup protons) requires that there be rapid exchange of CTAB between the inner and outer portion of this bilayer structure on the NMR time scale resulting in an average chemical shift. This required averaging has not been discussed in previous NMR studies of CTAB-coated nanoparticles.[34] Interestingly, recent molecular dynamics simulations of cetyltrimethylammonium (CTA^+)-capped Ag nanoparticles revealed a bilayer structure with a high degree of curvature of chain disorder, and that the CTA^+ molecules were not fixed, but readily exchanged between different portions of the bilayer structure.[39]

The ^{1}H NMR chemical shifts for the POPC and the POPC−gold nanorod composite are almost identical and show very little variation due to the interaction between the PC and the nanorod. The initial line widths of the POPC SUV range between 10 and 95 Hz and are consistent with the 34 nm radius determined from light scattering. In the POPC−gold nanorod sample, the ^{1}H NMR line widths increase consistent with adsorption to the Au nanorod (see Table 1). The large line width in-

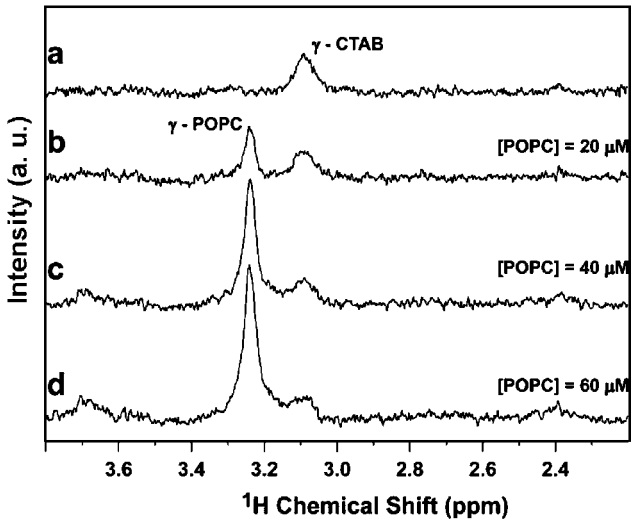

Figure 3. ^{1}H NMR spectra of the CTAB-protected gold nanorods during the titration with POPC SUV solution.

crease, especially for the broad component of the γ-methyl resonance, may obscure subtle chemical shift changes. Inspection of Figure 3d reveals no distinct residual CTAB−gold nanorod resonances in the POPC−gold nanorod sample. While many of the ^{1}H NMR resonances overlap in the CTAB and POPC spectra, the γ-methyl resonance for CTAB associated with the gold surface ($\delta = 3.11$ ppm) should be clearly distinguishable. In addition, a resonance for γ-methyl in unbound CTAB within a micelle structure (with a 10 Hz line width) was not observed. The last observation is not unexpected as this sample was centrifuged after the addition of excess POPC to remove any unbound CTAB and POPC species. Figure 3d also reveals an overlapping broad and narrow spectral component, most notably in the γ-methyl resonance and the main-chain CH_2 resonance. These overlapping resonances have been deconvoluted and reveal ~71−74% of the broad component (Table 1). It is known that for POPC the evolution of SUV to large unilamellar vesicles (LUV) or multilamellar vesicles (MLV) produces a dramatic increase in the ^{1}H NMR line width ultimately leading to broad and unresolved solution ^{1}H NMR spectra. This change in the vesicle size is also supported by the disappearance of the glycerol backbone signal (g_1, g_2, and g_3) due to increasing residual dipolar coupling with increasing vesicle size. The ^{1}H NMR spectra of the CTAB−gold nanorod mixture immediately following addition of excess POPC revealed only resonances with narrow line widths (spectrum not shown). Following centrifugation, the observation of a broad spectral component in the ^{1}H NMR spectrum shows that the structure of the POPC associated with the gold nanorods has changed and is no longer a simple SUV. In addition, this 1000-fold excess of POPC SUVs appears to have removed a large fraction of the CTAB from the nanorod surface since the CTAB γ-methyl protons are no longer observed in the POPC−gold nanorod spectra.

Additional insight into the interaction of POPC with the CTAB/nanorod composite can be obtained by following the ^{1}H NMR spectra during the titration of POPC at low concentrations. Figure 3 shows an expansion of the γ-methyl region during this process. Initially, only the γ-methyl resonance of the Au surface-bound CTAB is observed at ~3.1 ppm. Titrating the POPC concentration to 20 μM produces a new resonance at ~3.26 ppm resulting from the γ-methyl protons of POPC. By integration of these two resonances, the initial concentration of the CTAB on the nanorods is calculated to be ~30 μM, consistent with the 40 μM CTAB concentration estimation based on particle size and surface coverage. With the initial 20 μM POPC, there is a ~35% reduction in the intensity of the γ-methyl proton signal for the surface-bound CTAB. Titration to 60 μM POPC further reduces the γ-methyl of the surface-bound CTAB signal down to 35% of the initial intensity, with a corresponding increase in the in the γ-methyl signal arising from the POPC. It should be noted that using 60 μM (8-fold molar excess) POPC does not completely remove the surface-bound CTAB (~35% residual CTAB remaining). However, as shown in Figure 2d, using 1000-fold molar excess, POPC does remove most of the residual CTAB from the gold nanorod surface, noted by the complete disappearance of the CTAB γ-methyl protons in the POPC−gold nanorod spectrum (approximately <10% residual CTAB).

Detailed kinetic and equilibrium studies of this exchange were not pursued in the current investigation, and for the preparation of the POPC-coated nanorods, an excess of POPC was always utilized. However, incubation of this titrated POPC/CTAB/nanorod sample (Figure 3d) for 12 h at 47 °C did not produce any additional spectral changes, arguing that a slow kinetic release of CTAB from the surface during this time frame was not occurring. Moreover, equilibrium constants for the CTAB/POPC exchange process can be estimated using the integrated concentrations of CTAB and POPC measured in the NMR titration. For the 60 μM POPC addition, assuming random exchange in both the inner and outer bilayer leaflet, $K = 0.5$. Assuming there is thermodynamic preference for headgroup interaction at the gold nanorod surface (lower free energy) and random exchange for the outer leaflet only, then the equilibrium constant for the inner leaflet is $K = 0.3$. These two scenarios suggest the equilibrium is slightly in favor of the CTAB−gold nanorod interaction at 60 μM POPC, which is consistent with the observation of 35% residual CTAB (Figure 3d). However, when 10 mM POPC is used to exchange with CTAB, the equilibrium is largely in favor of POPC displacing CTAB, consistent with the observation of <10% residual CTAB (Figure 2d). These NMR results clearly demonstrate that the nanorod surface-bound CTAB is displaced by the addition of POPC.

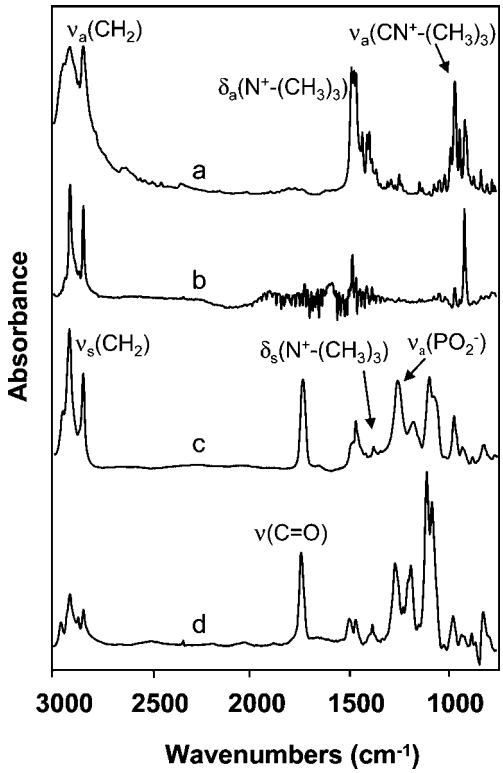

Figure 4. FT-IR spectra of (a) CTAB, (b) CTAB−gold nanorods, (c) POPC, and (d) POPC−gold nanorods.

During the POPC titration, no clear spectral signature of free CTAB being release into solution was observed. The titration samples were not centrifuged or separated between POPC additions, such that the CTAB molecules are still present in the mixture. The resonance for CTAB within a micelle structure would appear at ~3.16 ppm (Table 1) as a shoulder to the γ-methyl resonance of POPC with a line width of ~10 Hz but was not observed. On the other hand, the nominal concentration of released CTAB in this titration experiment (~30 μM) is well below the CMC of CTAB (900 μM) and therefore could exist as a free molecular species. It is known that ^{1}H NMR chemical shift of the CTAB γ-methyl headgroup changes dramatically below the CMC. For CTAB concentrations in solution between 10 and 20 μM, the chemical shift would be between 3.24 and 3.27 ppm.[40] This would place the free CTAB signal directly under the POPC γ-headgroup signal and would be unobservable. Similarly, mixing of CTAB micelles with POPC SUV results in an increased frequency shift of the CTAB γ-methyl signal from ~3.16 to ~3.2, such that the free CTAB resonance may be obscured by the POPC. As stated above, POPC−gold nanorods were prepared using 1000-fold excess of POPC vesicles for all other experiments in an effort to displace the maximum amount of CTAB from the nanorod surface.

As a compliment to the ^{1}H NMR data, FT-IR spectra were acquired for CTAB− and POPC−gold nanorod composites. Figure 4 shows FT-IR spectra of neat (solid) CTAB, CTAB−gold nanorods, neat (solid) POPC, and POPC−gold nanorods. The peak frequency assignments are given in Table 2.[41−46] While there are overlapping vibrational modes in the IR spectra of CTAB and POPC making it more difficult to qualitatively follow the exchange process than in ^{1}H NMR, there are a number of distinct spectral differences in the fingerprint region (1000−1800 cm^{-1}). For POPC−gold nanorods, carbonyl ν(C═O) (1743 cm^{-1}); phosphate $\nu_a(PO_2^-)$ (1264 cm^{-1}), $\nu_s(PO_2^-)$ (1104 cm^{-1}); and ester modes ν_a(C−O−C) (1186 cm^{-1}), ν_s(C−O−C) (1075 cm^{-1}) are readily observable (Figure 4d). The presence of these modes suggests POPC modification of the gold nanorod surface and is in good agreement with the ^{1}H NMR results. Quaternary ammonium $\nu_s(CN^+-(CH_3)_3)$ (~910 cm^{-1}) and $\nu_a(CN^+-(CH_3)_3)$ (~970 cm^{-1}) modes are observed for both CTAB− and POPC−gold nanorods (Figure 4b,d). Both spectra in Figure 4b,d were acquired using the same nanorod sample, before and after POPC modification, just as in the NMR experiments. The IR data suggest that POPC dominates the interaction with the gold nanorods just as was observed with the NMR measurements when prepared with a large excess POPC. Any residual CTAB adsorbed to the nanorod surface or incorporated into the POPC bilayer is masked by overlapping POPC vibrational modes or is present at immeasurable quantities by FT-IR.

The frequencies and relative intensities of the headgroup vibrational modes for CTAB and choline lipids analogous to POPC are known to be indicators of structure and environment, especially in micelles, vesicles, or supported bilayers.[45−48] For CTAB−gold nanorods, the asymmetric quaternary ammonium N−C bending mode, $\delta_a(N^+-(CH_3)_3)$, is observed at 1481 cm^{-1}; however, the asymmetric N−C bend, $\delta_s(N^+-(CH_3)_3)$ (~1395

TABLE 2. Peak Frequencies and Assignments for CTAB, CTAB−Gold Nanorods, POPC, and POPC−Gold Nanorods

peak frequency (cm^{-1})				
CTAB	CTAB−Au NRs[b]	POPC	POPC−Au NRs[c]	assignment[a]
2950	2944sh	2957	2964	$\nu_a(CH_3)$
2917	2917	2922	2918	$\nu_a(CH_2)$
2869	2870	2873	2874	$\nu_s(CH_3)$
2850	2851	2852	2848	$\nu_s(CH_2)$
—[d]	—	1739	1743	ν(C═O)
1486	—	1492sh[e]	1497	$\delta_a(N^+-(CH_3)_3)$
1473	1481	1482	1491	$\delta_a(N^+-(CH_3)_3)$
1461	1463	1467	1468	$\delta(CH_2)$ scissor
1394	—	—	—	$\delta_s(N^+-(CH_3)_3)$
—	1381[f]	1378	1379	$\delta_s(C-(CH_3)_3)$
—	—	1253	1264	$\nu_a(PO_2^-)$
—	—	1175	1186	ν_a(C−O−C)
—	—	1092	1104	$\nu_s(PO_2^-)$
—	—	1071	1075	ν_s(C−O−C)
962	962	968	970	$\nu_a(CN^+-(CH_3)_3)$
910	910	923	925	$\nu_s(CN^+-(CH_3)_3)$

[a]Assignments made from refs 41−46; ν = stretch; δ = bend or scissor. [b]CTAB−gold nanorods. [c]POPC−gold nanorods. [d]Not observed [e]Shoulder. [f]The $\delta_s(C-(CH_3)_3)$ mode for CTAB−gold nanorods is buried in the streaked baseline.

cm^{-1}), is too weak to be observed in the streaked baseline from ~1400 to 1700 cm^{-1} due to residual moisture in these samples prepared from aqueous solution. The observation of the N−C bending modes suggests that the quaternary ammonium headgroup of CTAB is strongly associated with the gold nanorod surface.[45,47,48] Moreover, the suppression of the asymmetric C−N−C stretch relative to the symmetric C−N−C stretch, $\nu_a(CN^+-(CH_3)_3)$ (962 cm^{-1}) and $\nu_s(CN^+-(CH_3)_3)$ (910 cm^{-1}), in CTAB−gold nanorods is also consistent with surface-bound quaternary ammonium groups.[48] These observations are in good agreement with the ^1H NMR data that show a chemical shift in the γ-methyl protons when CTAB interacts with the gold nanorod surface (Table 1). For POPC−gold nanorods, the $\delta_a(N^+-(CH_3)_3)$ is observed at 1491 cm^{-1}, which indicates interaction between the choline headgroup and the gold nanorod surface.[45] In addition, the decrease in intensity of the $\delta(CH_2)$ scissor mode at 1468 cm^{-1} relative to the $\delta_a(N^+-(CH_3)_3)$ mode at 1491 cm^{-1} indicates a well-ordered liquid crystalline lipid bilayer analogous to observations for DMPC and DPPC.[45,48] The red shift observed in $\nu_a(PO_2^-)$ and $\nu_s(PO_2^-)$ frequencies from 1253 and 1092 cm^{-1}, respectively, in bulk POPC to 1264 and 1104 cm^{-1} in POPC−gold nanorods suggests electrostatic interactions between negatively charged phosphate and positively charged quaternary ammonium moieties of adjacent lipid headgroups, analogous to observations made for supported DMPC bilayers on titania surfaces.[46,48] Moreover, the observation of the $\nu_s(CN^+-(CH_3)_3)$ mode at 925 cm^{-1} for POPC−gold nanorods suggests that the quaternary ammonium headgroup is in a trans conformation (N−C−C−O), facilitating electrostatic interactions between adjacent lipid molecules.[49] In contrast, the $\nu_s(CN^+-(CH_3)_3)$ mode for CTAB−gold nanorods is observed at 910 cm^{-1}, suggesting a gauche conformation of the headgroup (N−C−C−C) at the gold surface giving rise to perhaps a less well-packed or more fluxional stabilizing surfactant bilayer than the POPC lipid bilayer.[49] In general, the IR spectrum for POPC−gold nanorods suggests that POPC is strongly associated with the nanorod surface and exists in a bilayer-type structure, which is in good agreement with the ^1H NMR results also consistent with previous FT-IR characterization of DMPC and DPPC supported lipid bilayers.

Changing the surface species on gold nanorods from CTAB to POPC has a significant impact on surface functionality. This impact is reflected in ζ-potential measurements that have been obtained on both types of nanorods to measure surface charge as a function of solution pH. As expected for surface termination by a quaternary amine, the ζ-potential of CTAB-coated nanorods is large, positive (+39 mV), and independent of pH. While POPC-coated nanorods exhibit a comparable surface charge at low pH (with a ζ-potential of +30 mV), the surface charge decreases with pH to a steady state value of around 10 mV for pH 7 and above. This pH-dependent surface charge is associated with the deprotonation of the phosphate group that lies below the quaternary ammonium group in POPC. In solution, this phosphate group is reported to have a pK_a of around 1.[50,51] With this pK_a, total deprotonation of the phosphate group would be expected to occur at pH values above pH 3, creating a neutral zwitterion (*i.e.*, a phosphate anion adjacent to the quaternary ammonium cation).[50,51] Neutralization of the surface charge should minimize electrostatic repulsion between nanorods, allowing them to aggregate. Relative to POPC dissolved in solution, the ζ-potential *versus* pH curve on our gold nanorods is broader, shifted to higher pH, and contains residual positive charge even at high pH (Figure 5). The broadening in the pH response and the shift to higher apparent pK_a values are often seen in polyelectrolytes (PEs) and self-assembled monolayers on surfaces (gold, silicon, *etc.*) and have been attributed to chain−chain and chain−substrate interactions.[9,52−55] We believe that the slight residual positive charge in the POPC-coated rods is associated with the retention of residual CTAB within the POPC layer. Previous studies have shown that, when POPC vesicles are exposed to CTAB, the CTAB can insert into the POPC, resulting in a positive ζ-potential that saturates at a CTAB concentration in the POPC of around 4 mol %.[56] While we cannot determine the exact CTAB concentration from the ζ-potential value, our NMR and FT-IR results combined with the ζ-potential results suggest that the residual concentration is somewhere between 4 and 10 mol %.

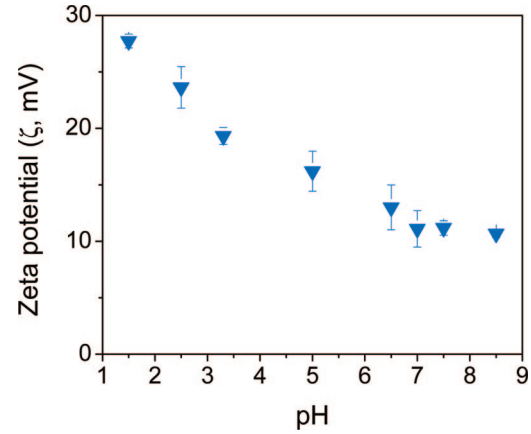

Figure 5. Plot of ζ-potential as a function of pH for zwitterionic POPC−gold nanorods. Error bars represent one standard deviation.

Lipid−Gold Nanorod Self-Assembly. It is interesting to consider what effect the pH-dependent surface charge of POPC−gold nanorods has on nanorod self-assembly. The expectation is that repulsive forces between cationic CTAB nanorods would keep them isolated. The same would be expected for POPC−gold nanorods at low pH. However, at higher pH, repulsive cationic forces are diminished and one would expect some degree of

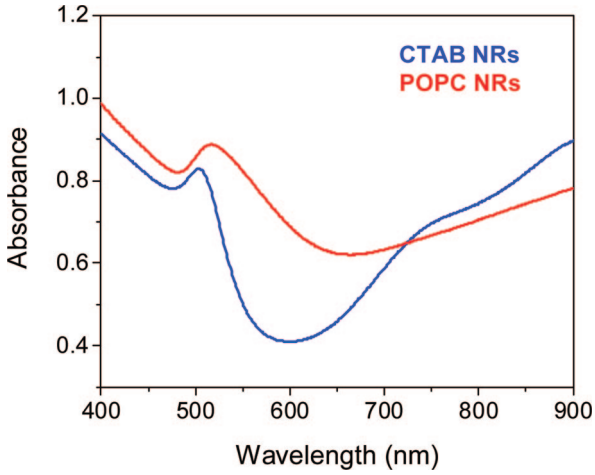

Figure 6. Absorption spectra of CTAB−gold nanorods (blue trace) and POPC−gold nanorods (red trace) in H_2O.

self-assembly with a preference for side-to-side assembly in order to maximize van der Waals interactions.

Figure 6 shows the absorption spectra of CTAB− and POPC−gold nanorods at pH 7 in H_2O. In this range from 400 to 900 nm, only the transverse plasmon absorption band is observed (the longitudinal plasmon absorption for aspect ratio 18 gold nanorods is ~1800 nm).[23] For CTAB−gold nanorods, the transverse plasmon absorption is observed at 503 nm, while the absorption maximum for POPC−gold nanorods is observed at 517 nm and has a broad, red-shifted asymmetric shape. Red-shifting transverse plasmon absorption can result from a number of physical changes to nanorods including increasing nanorod diameter,[57] increasing local refractive index,[58] or nanorod plasmon coupling through nanorod−nanorod interactions.[59] Since the nanorod size does not change and the refractive index of POPC is assumed to be comparable to CTAB, then the shift and broadening of the transverse plasmon band in POPC−gold nanorods could be attributed to plasmon coupling between nanorods. This suggests that POPC−gold nanorods are self-assembled side-to-side in solution, causing plasmon coupling and a red shift in the transverse absorption.

Figure 7a−d shows representative TEM images of CTAB-protected gold nanorods (Figure 7a,b) and POPC−gold nanorods (Figure 7c,d). In the CTAB−gold nanorod images, nanorods are well-dispersed and assemble onto the TEM grid in a disordered pattern with a statistical preference for end-to-end and end-to-side interactions over side-to-side. The occurrence of each interaction was counted for a total sample size of >500 nanorods and plotted in Figure 8. The diminished occurrence of side-to-side interactions is likely due to electrostatic repulsion between strongly cationic (+39.4 ± 2.8 mV) CTAB nanorods. Given the high radius of curvature at the nanorod end, it is possible that the distal portion of CTAB molecules are spaced further apart at the nanorod ends than at the sides or may even exist as monolayers, leading to less electrostatic charge and repulsion at the nanorod ends compared to the sides. While it is difficult to experimentally prove that the ζ-potential at the end of a CTAB−gold nanorod is different than at the side, it is well-known that there are significant differences between the ends and side of CTAB−gold nanorods in terms of their crystallography,[60] assembly,[2−4] and chemical reactivity.[2,61] TEM samples prepared from these 1 × 10^{10} particles/mL concentration nanorod solutions do not assemble into well-defined structures, but liquid crystalline nanorod assemblies can be prepared using CTAB nanorods at higher concentrations, the addition of electrolyte, or by control of solvent evaporation during sample preparation.[12−14,62]

POPC nanorods assemble into side-to-side 2D structures with short-range order, as shown in Figures 6 and 7. By replacing the CTAB surface group with a POPC lipid, the ζ-potential of the composite decreases from +39.4 ± 2.8 mV (CTAB) to +11.1 ± 1.6 mV (POPC) at pH 7. This significant decrease in ζ-potential decreases electrostatic repulsion between nanorods. Moreover, the presence of both cationic and anionic functionality at the headgroup of POPC could result in charge pairing between adjacent nanorods to direct the observed side-to-side assembly. It should be noted that CTAB−

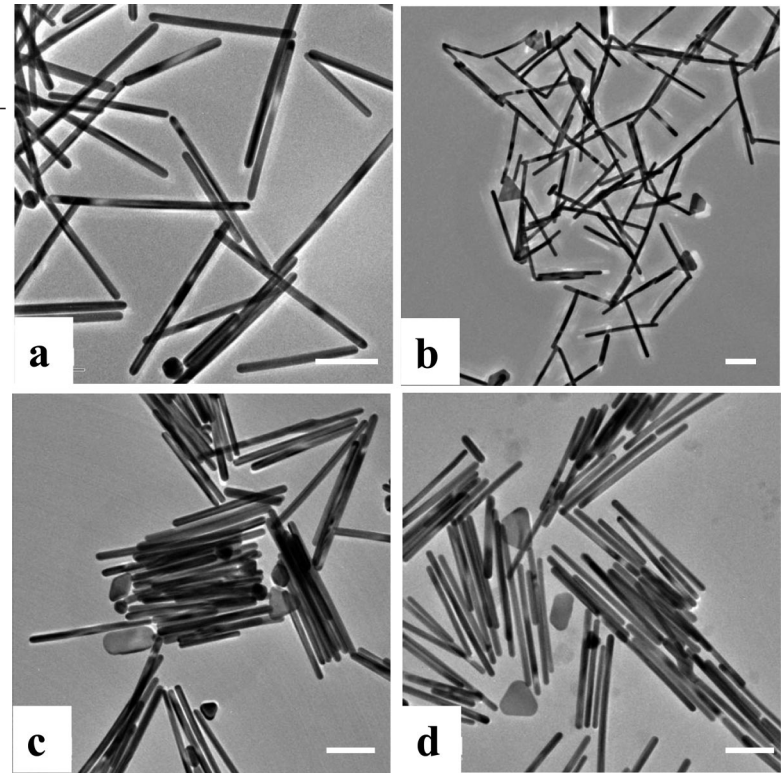

Figure 7. Representative TEM images of (a and b) as-prepared CTAB−gold nanorods and (c and d) POPC−gold nanorods at pH 7.0. Scale bar represents 100 nm.

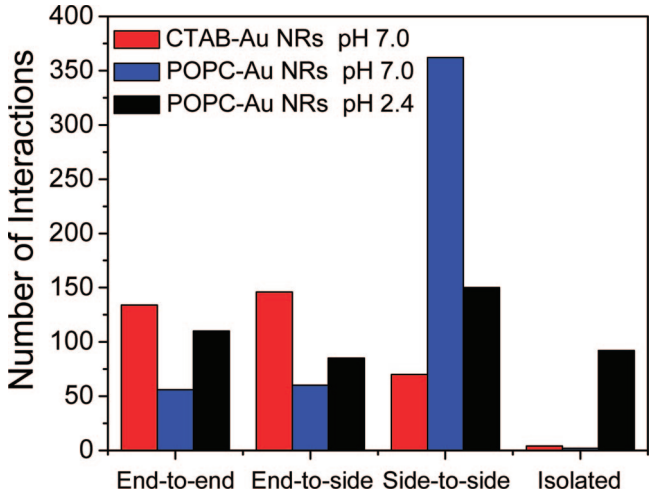

Figure 8. Number of occurrences of nanorod−nanorod interactions in a ~400 nanorod sample population including end-to-end, end-to-side, and side-to-side for CTAB−gold nanorods (red), POPC−gold nanorods at pH 7.0 (blue), and POPC−gold nanorods at pH 2.4 (black).

and POPC−gold nanorod TEM samples were prepared by both solvent evaporation and emersion from bulk solution techniques. The results from both preparations were identical, suggesting that the assembly of POPC−gold nanorods was not a solvent evaporation or grid preparation effect, but rather a function of the composite surface chemistry.

As shown in Figure 5, the ζ-potential of POPC−gold nanorods was pH-dependent. Then, there is an expectation that POPC−gold nanorod assembly could also be pH-dependent if, in fact, electrostatic interactions contribute to their self-assembly. Figure 9 shows TEM images of POPC−gold nanorods at pH 7.0 and 2.4. In this representative image at pH 2.4, there were significantly fewer nanorods self-assembled side-to-side than at pH 7.0 with a large fraction of isolated nanorods. In fact, the occurrence of these interactions for the POPC−gold nanorod sample at pH 2.4 was recorded and shown in Figure 8. As the solution pH decreases from 7.0 to 2.4, the ζ-potential of the POPC composite increases from $+11.1 \pm 1.6$ to $+23.7 \pm 1.8$ mV, increasing electrostatic repulsion between POPC−gold nanorods. The result was that we observed nanorod disassembly at low pH compared to at pH 7.0 (Figure 9). This not only provides evidence to support the argument that electrostatic interactions govern nanorod assembly but also gives insight into how these lipid nanorod composites could be reconfigured or their assembly/disassembly may be cycled by tuning environmental parameters, such as pH.

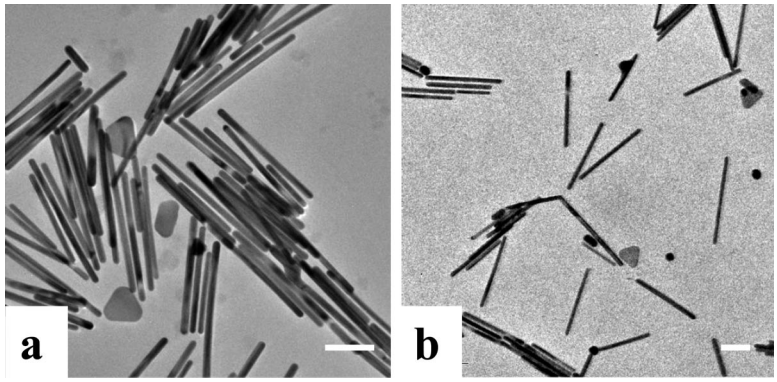

Figure 9. Representative TEM images of POPC−gold nanorods at (a) pH 7.0 and (b) pH 2.4. Scale bar represents 100 nm.

DISCUSSION

While individual gold nanorods exhibit interesting electrical and optical properties, these nanoparticles also represent important building blocks for nanocomposites due to their anisotropic shapes. Previous research has shown that a wide range of architectures can be assembled from nanorods depending on the size and shape of the rods as well as deposition conditions. Such structures include "one dimensional" end-to-end chains, rings, and open end-to-end networks at one extreme to densely packed side-to-side liquid crystalline arrays at the other extreme.[2−4,60−62] However, to date, most structural variations have been achieved *via* physical means (*e.g.*, particle shape, solution concentration, or the application of pressure in Langmuir trough arrays). We are interested in exploring the extent to which such variations can be achieved and even programmed *via* chemical means (*e.g.*, surface functionalization). The phospholipids represent a rich class of potential capping agents that allow for extensive variations in the size, shape, and headgroup chemistry for terminating gold surfaces. Not only can the phospholipids control how nanorods interact with each other but also they can decorate nanorod surfaces with functional groups that can be used to couple to other elements in multifunctional composites or environmental species (*e.g.*, for sensors). This paper represents the first demonstration that phospholipids can be incorporated onto the surfaces of gold nanorods and that such incorporation mediates assembly phenomena.

Some of the key issues associated with the functionalization of nanorods and the impact of that functionalization on assembly are highlighted by examining the details of what is known regarding (1) the structure and properties of the "native" capping agent CTAB, (2) how the capping agent might be modified and/or replaced by phospholipids, and (3) what structures and properties might be expected once the modification or replacement has taken place. First, while CTAB is a simple surfactant with a hydrocarbon tail and a tetramethylammonium ion headgroup, previous studies of CTAB on gold suggest that the CTAB actually forms a bilayer or even multilayer structures on the nanorod surfaces (Figure 10). In such structures, it is postulated that the layer at the immediate surface has the methylamine group adjacent to the gold, with the hydrocarbon tail

projecting away from the surface. As in lipid bilayers, the second layer is inverted with the hydrocarbon tails contacting the tails in the first layer, allowing the water/particle interface to be terminated with the hydrophilic trimethylammonium group. The typical interparticle spacing of 9.0 nm in close-packed arrays of CTAB-coated nanorods relative to the extended CTAB chain length of 2.2 nm is consistent with contact between two such lipid bilayer structures. However, in some instances, packing can induce closer approach distances (3.4 nm), suggesting that, once all water is expelled between the particles, two adjacent bilayers can coalesce into a single bilayer in which the hydrocarbon chains on one particle are interleaved with those on the adjacent particle (Figure 10).

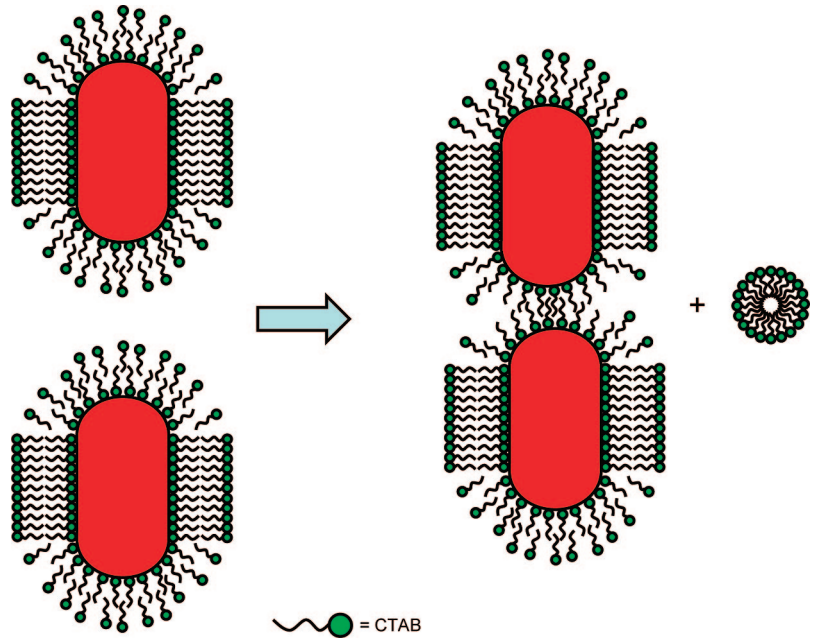

Figure 10. Cartoon showing a mechanism for the end-to-end interaction between two CTAB−gold nanorods.

A further complication is associated with how CTAB capping agents behave at the ends of the nanorods. It is known that the chemical and physical properties of nanorod ends can be substantially different than those of the sides.[2,61] For the specific case of CTAB, this and previous studies have shown that, while particle sides do not stick to each other due to electrostatic repulsion associated with the trimethylammonium groups, the ends of the rods can actually be quite sticky (Figures 7 and 8). The lack of repulsion on chain ends favors the end-to-end and end-to-side agglomerate structures reported here and elsewhere.[61] The lack of repulsion on chain ends can be rationalized by a model in which the high radius of curvature on rod ends leads to a spreading of the chains and a more fluxional, loosely packed structure.[56,63] It is postulated that this more open structure not only has a lower charge density but also is sufficiently fluxional to promote the loss of a sufficient number of CTAB molecules to promote the formation of the interdigitated bilayer shown in Figure 10 upon interparticle contact. This propensity for end-to-end interaction is further supported by the fact that centrifuging CTAB−gold nanorods at high speeds or for extended periods of time causes nanorods to fuse together either end-to end or end-to side (Supporting Information Figure 1S).

Fluxionality and molecular exchange are undoubtedly important not only to the behavior of the CTAB capping agent but also for the exchange of CTAB by phospholipids and other surfactants. As shown in Figure 11, there could be multiple responses when a CTAB-coated nanorod is exposed to a phospholipid-containing solution: (1) there could be no exchange, provided that CTAB has a much higher affinity for the gold than the phospholipids; (2) there could be a partial exchange of CTAB by phospholipids, with one potential end state being a bilayer structure with an inner leaflet of CTAB and an outer leaflet of phospholipids; and (3) there could be a complete and total exchange, resulting in a capping layer consisting of a pure phospholipid. Our NMR, IR, and ζ-potential results indicate that exchange is essentially complete when a large excess of phospholipid is present, but some residual CTAB (~4 mol %) remains incorporated in the POPC bilayer. Equilibrium constants estimated for the CTAB/POPC exchange process show that both molecules have a comparable affinity for adsorption onto gold due to the trimethylammonium terminal group that is shared by both molecules. We suspect that exchange of CTAB by a wide range of phospholipid groups should be possible under mild exchange conditions (*e.g.*, solution ex-

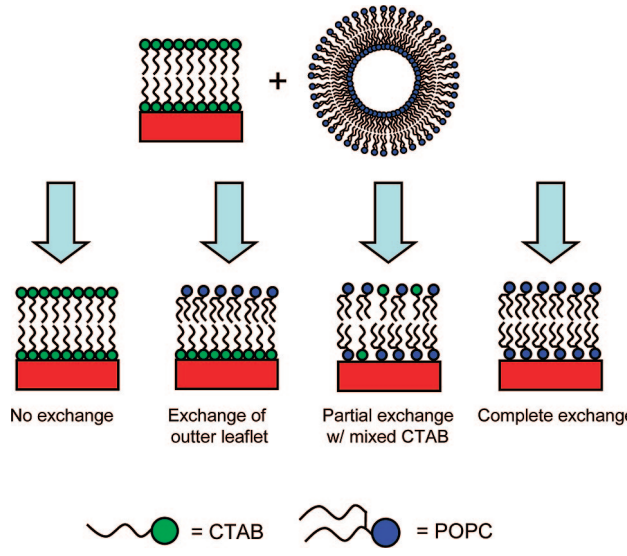

Figure 11. Illustration of the possible results for the addition of POPC vesicles with CTAB−gold nanorods showing no exchange, exchange of the upper leaflet, partial exchange forming a mixed CTAB/POPC bilayer, and complete exchange.

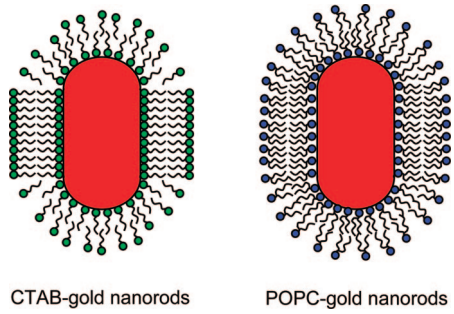

Figure 12. Cartoon showing the possible differences between CTAB and POPC bilayers on gold nanorods, notably at highly curved nanorod ends.

change in an excess of phospholipids at room temperature).

Although the phospholipids can cap gold nanoparticles, the agglomeration properties of the capped particles suggest that POPC layers are not only chemically different that CTAB but are structurally different, as well. The chemical differences associated with having an ionizable phosphate group in addition to the terminal trimethylamine group are clearly apparent in both ζ-potential measurements and the transmission electron micrographs of agglomerate structures. As might be expected, deprotonation of the phosphate group at higher pH values transforms the terminal group from a cationic site into a near-neutral zwitterion, largely eliminating electrostatic repulsion between the particles and allowing side-to-side agglomerates to form. The physical differences between CTAB and POPC are apparent in the low pH regime in which both capping layers have comparable surface charges. In contrast to CTAB, which has a tendency to favor end-to-end and end-to-side agglomeration, POPC at high pH inhibits all agglomeration, favoring the formation of isolated nanorods (Figure 8). This observation suggests that POPC is an effective capping agent on the ends as well as the sides of the rods. This is illustrated in Figure 12, where we believe that the lipid bilayer structure is preserved on the nanorod ends, in contrast to the unstable or partially missing bilayers inferred for CTAB. The enhanced stability of POPC bilayers in the high curvature regime in rod ends may be associated with the presence of a more bulky headgroup or due to stabilization associated with having two hydrocarbon tails instead of just one (like a "chelate effect"). POPC bilayer stability is supported by the strong intermolecular interactions between POPC molecules of the bilayer and interactions between the POPC headgroup with the gold nanorod surface observed in the FT-IR spectra (Figure 4). Future studies with a wide range of different phospholipids will be required to sort out the relative importance of headgroup and tail geometries on behavior. However, we anticipate that, for mixed phospholipids systems, bulky headgroups will have a preference for rod ends, opening up the possibility of creating "Janus" particles in which the end and sides of the nanorods can be decorated with different functional groups.

CONCLUSIONS

POPC−gold nanorod composites were prepared by immobilizing liposomes onto the surface of CTAB-protected gold nanorods. The synthesis of lipid−gold nanorod composites was confirmed by ^{1}H NMR and FT-IR spectroscopies, showing a strong association between the lipid and the gold nanorod surface and no detectable residual CTAB surfactant in the lipid nanorod composite samples. While these data indicate that CTAB has been displaced from the nanorod surface, additional experiments to measure the kinetics and binding strength during the surfactant−lipid exchange reaction are currently underway in an effort to better understand this process. POPC−gold nanorod composites have zwitterionic functionality making their ζ-potential pH-dependent and ~30 mV less positive than as-prepared CTAB−gold nanorods at pH 7.0. Electrostatic repulsion between cationic CTAB−gold nanorods directs their assembly into disordered arrangements favoring end-to-end or end-to-side interactions. POPC−gold nanorod composites self-assemble side-to-side with short-range order at pH 7.0, and these structures can disassemble as their surface ζ-potential becomes more cationic and repulsive with decreasing pH. This work describes a procedure for modifying the surface of gold nanorods with phospholipids. This process expands the range of different functional groups that can be used to modify nanorods from the intercalation of single components to the incorporation of mixed bilayers. Moreover, phospholipids can be selected to include phase separation to the ends *versus* the sides of the nanorods based on lipid shape. This combined work will be focused toward driving research toward switchable or reconfigurable surfaces and materials.

EXPERIMENTAL SECTION

Materials. Chloroauric acid was purchased from Alfa Aesar. Sodium borohydride, ascorbic acid, and chloroform were purchased from Aldrich. Cetyltrimethylammonium bromide (CTAB) was purchased from Sigma. L-α-Phosphatidylcholine (egg yolk, egg-PC) and 1-palmitoyl-2-oleoyl-*sn*-glycero-3-phosphocholine (POPC) were purchased from Avanti Polar Lipids. As both lipid samples contained essentially the same phospholipid, with egg-PC containing a small fraction of multiunsaturated chains, other PC lipids, isomers, and impurities, and both yielded nearly identical results in the experiments, we will simply refer to them as POPC. Aqueous solutions used for lipid vesicles were prepared from water purified through a Barnstead type D4700 NANOpure Analytical Deionization System with ORGANICfree cartridge registering an 18.0 MΩ · cm resistance. Deionized ultrafiltered (DIUF) water used for all other experiments was purchased from Fisher Scientific.

Gold Nanorod Preparation. Aspect ratio 18 gold nanorods (307 ± 61 nm in length and 17 ± 2 nm in width) were prepared from a seed-mediated approach described by Jana *et al.*[23,24] CTAB-protected gold seed particles were prepared by the chemical reduction of a 2.5×10^{-4} M $HAuCl_4$ solution in 0.1 M CTAB by the addition 0.6 mL of ice-cold 0.01 M $NaBH_4$ while stirring rapidly for 2 min. Gold nanorods were prepared using a three-step growth procedure. "Growth" solution was prepared in three vessels labeled **A**, **B**, and **C** by adding 9 mL of 2.5×10^{-4} M $HAuCl_4$ in 0.1 M CTAB to **A** and **B** and 90 mL of the same solution to **C**. To the growth solution was added 50 μL of 0.1 M ascorbic acid to **A** and **B**, and 0.5 mL of 0.1 M ascorbic acid was added to **C** to reduce Au^{3+} to Au^{1+}. Further reduction of Au^{1+} to Au^0 was achieved by addition 1 mL of as-prepared CTAB-protected gold seeds to **A**. After 15 s, 1 mL of **A** was added to growth solution **B**. After 30 s, all of the growth solution **B** was added to **C**. Solution **C** was aged for >12 h, after which it contained a mixture of gold nanorods and nanospheres. Nanorods were removed from other shapes by gently warming the solution to redissolve precipitated CTAB and decanting off the solution containing undesired shapes and redispersing CTAB nanorods in ~5 mL of deionized water. The resulting solution contained approximately 10^{10} nanorods/mL determined by absorption spectroscopy using a molar extinction coefficient of 1×10^9 M^{-1} cm^{-1} for the transverse plasmon band.[29]

Liposome Preparation. Dried POPC lipid films were prepared by evaporating 5.0 mL of a 20 mM chloroform solution of lipid onto the sides of a conical vial using a rotary evaporator. The dried films were then further dried under high vacuum overnight to remove traces of the organic solvent. The film was then hydrated in either 5.0 mL of MOPS buffer solution (0.02 M 4-morpholinopropanesulfonic acid and 0.1 M NaCl adjusted to pH 7.4 with aqueous 10% NaOH solution) or in pure water at 40 °C for 1 h. Periodic vortexing of the sample suspended the lipid films into solution, which was then degassed with N_2 gas for several minutes followed by sonication with a 3 mm probe tip at ~10 W power under N_2 gas. Sonication was performed in 4 min cycles with 4 min resting and cooling between each cycle for a total of 32 min at room temperature. The translucent solution was then centrifuged for 20 min at 16 000*g*, and the supernatant was filtered through a 0.22 μm filter and then diluted to a volume of 10 mL to yield a nominal lipid concentration of 10 mM. Resulting POPC small unilamelar vesicles (SUVs) have an average hydrodynamic radius of 34 nm with a polydispersity of 22 nm determined by dynamic light scattering.

Lipid Nanorod Preparation. Lipid nanorod composites were prepared by centrifuging 15 mL of a 10^{10} nanorods/mL solution at 6000 rpm for 5 min, redispersing them in deionized water, followed by a second centrifugation step at 5000 rpm for 8 min in order to remove excess CTAB surfactant. The final nanorod pellet was resdispersed in 0.75 mL of deionized water. A 2 mL aliquot of 10 mM POPC SUVs was added to 0.75 mL of gold nanorods and homogenized with a pipet. After 12 h, POPC–gold nanorods were centrifuged at 4000 rpm for 8 min and redispersed in deionized water in order to remove unbound or excess lipid from solution. For the NMR experiments, all nanorod samples were centrifuged, separated, and then redispersed in D_2O.

Instrumentation. Zeta potential (ζ-potential) measurements were made using a Malvern Zetasizer Nano ZS zeta potential/light scattering instrument. Transmission electron microscopy (TEM) images were acquired using a JEOL 2010 high-resolution transmission electron microscope. TEM samples were prepared by either immersing Formvar/carbon-coated copper grids into a ~0.2 mL nanoparticle solution drop for 20 min or dropping 5 μL of nanoparticle solution onto a grid and allowing it to dry under ambient conditions. Absorption spectra used to quantify the number of gold nanorods in solution were acquired using a Cary 600i UV–vis–NIR spectrophotometer. The ^{1}H NMR measurements were obtained on a Bruker Avance600 instrument at 600.12 MHz using a 5 mm BB solution probe. Reflectance FT-IR spectra were obtained using p-polarized light at an incident angle of 85° with respect to the surface normal using a Harrick Seagull variable reflection accessory (Harrick). All spectra are the average of 3000 scans of both the sample and the reference. Spectra were acquired at 2 cm^{-1} resolution and Blackman-Harris apodization using a liquid N_2-cooled MCT-D316 detector. Spectra are reported as $-\log(R/R_0)$, where R is the reflectance of the sample and R_0 is the reflectance of the reference.

Acknowledgment. The authors gratefully acknowledge the Department of Energy's Office of Basic Science for support of this work, and N.S. Bell for the use of the Malvern Zetasizer ζ-potential analyzer. Sandia is a multiprogram laboratory operated by Sandia Corporation, a Lockheed Martin Company, for the United States Department of Energy's National Nuclear Security Administration under Contract No. DE-AC04-94AL85000.

Supporting Information Available: Additional figure. This material is available free of charge *via* the Internet at http://pubs.acs.org.

REFERENCES AND NOTES

1. Murphy, C. J.; Sau, T. K.; Gole, A. M.; Orendorff, C. J.; Gao, J.; Gou, L.; Hunyadi, S. E.; Li, T. Anisotropic Metal Nanoparticles: Synthesis, Assembly, and Optical Applications. *J. Phys. Chem. B* **2005**, *109*, 13857–13870.
2. Caswell, K. K.; Wilson, J. N.; Bunz, U. H. F.; Murphy, C. J. Preferential End-to-End Assembly of Gold Nanorods by Biotin-Streptavidin Connectors. *J. Am. Chem. Soc.* **2003**, *125*, 13914–13915.
3. Chang, J.-Y.; Wu, H.; Chen, H.; Ling, Y.-C.; Tan, W. Oriented Assembly of Au Nanorods Using Biorecognition System. *Chem. Commun.* **2005**, 1092–1094.
4. Thomas, K. G.; Barazzouk, S.; Itty Ipe, B.; Joseph, S. T. S.; Kamat, P. V. Uniaxial Plasmon Coupling through Longitudinal Self-Assembly of Gold Nanorods. *J. Phys. Chem. B* **2004**, *108*, 13066–13068.
5. Dujardin, E.; Hsin, L.-B.; Wang, C. R. C.; Mann, S. DNA-Driven Self-Assembly of Gold Nanorods. *Chem. Commun.* **2001**, 1264–1265.
6. Ye, Y. H.; Mayer, T. S.; Khoo, I. C.; Divliansky, I. B.; Abrams, N.; Mallouk, T. E. Self-Assembly of Three-Dimensional Photonic-Crystals with Air-Core Line Defects. *J. Mater. Chem.* **2002**, *12*, 3637–3639.
7. Cai, L. T.; Skulason, H.; Kushmerick, J. G.; Pollack, S. K.; Naciri, J.; Shashidhar, R.; Allara, D. L.; Mallouk, T. E.; Mayer, T. S. Nanowire-Based Molecular Monolayer Junctions: Synthesis, Assembly, and Electrical Characterization. *J. Phys. Chem. B* **2004**, *108*, 2827–2832.
8. Park, H.-S.; Agarwal, A.; Kotov, N. A.; Lavrentovich, O. D. Controllable Side-by-Side and End-to-End Assembly of Au Nanorods by Lyotropic Chromonic Materials. *Langmuir* **2008**, *24*, 13833–1383.
9. Gole, A.; Murphy, C. J. Biotin-Streptavidin-Induced Aggregation of Gold Nanorods: Tuning Rod–Rod Orientation. *Langmuir* **2005**, *21*, 10756–10762.
10. Kim, F.; Kwan, S.; Akana, J.; Yang, P. Langmuir–Blodgett Nanorod Assembly. *J. Am. Chem. Soc.* **2001**, *123*, 4360–4361.
11. Tao, A.; Kim, F.; Hess, C.; Goldberger, J.; He, R.; Sun, Y.; Xia, Y.; Yang, P. Langmuir–Blodgett Silver Nanowire Monolayers for Molecular Sensing Using Surface-Enhanced Raman Spectroscopy. *Nano Lett.* **2003**, *3*, 1229–1233.
12. Nikoobakht, B.; Wang, Z. L.; El-Sayed, M. A. Self-Assembly of Gold Nanorods. *J. Phys. Chem. B* **2000**, *104*, 8635–8640.
13. Jana, N. R.; Gearheart, L. A.; Obare, S. A.; Johnson, C. J.; Edler, K. J.; Mann, S.; Murphy, C. J. Liquid Crystalline Assemblies of Ordered Gold Nanorods. *J. Mater. Chem.* **2002**, *12*, 2909–2912.
14. Jana, N. R. Shape Effect in Nanoparticle Self-Assembly. *Angew. Chem., Int. Ed.* **2004**, *43*, 1536–1540.
15. Obare, S. O.; Hollowell, R. E.; Murphy, C. J. Sensing Strategy for Lithium Ion Based on Gold Nanoparticles. *Langmuir* **2002**, *18*, 10407–10410.
16. Orendorff, C. J.; Hankins, P. L.; Murphy, C. J. pH-Triggered Assembly of Gold Nanorods. *Langmuir* **2005**, *21*, 2022–2026.

17. Barenholz, Y.; Cevc, G. *Structure and Properties of Membranes in Physical Chemistry of Biological Interfaces*; Baszkin, A., Norde, W., Eds.; Marcel Dekker Inc.: New York, 2000; pp 171−241.
18. Plant, A. L. Supported Hybrid Bilayer Membranes as Rugged Cell Membrane Mimics. *Langmuir* **1999**, *15*, 5128–5135.
19. Sackmann, E. Supported Membranes: Scientific and Practical Applications. *Science* **1996**, *271*, 43–45.
20. Keller, C. A.; Kasemo, B. Surface Specific Kinetics of Lipid Vesicle Adsorption Measured with a Quartz Crystal Microbalance. *Biophys. J.* **1998**, *75*, 1397−1402.
21. Cho, N.-J.; Cho, S.-J.; Cheong, K. H.; Glenn, J. S.; Frank, C. W. Employing an Amphipathic Viral Peptide to Create a Lipid Bilayer on Au and TiO_2. *J. Am. Chem. Soc.* **2007**, *129*, 10050–10051.
22. Takahashi, H.; Niidome, Y.; Niidome, T.; Kaneko, K.; Kawasaki, H.; Yamada, S. Modification of Gold Nanorods Using Phosphatidylcholine to Reduce Cytotoxicity. *Langmuir* **2006**, *22*, 2–5.
23. Jana, N. R.; Gearheart, L.; Murphy, C. J. Wet Chemical Synthesis of High Aspect Ratio Cylindrical Gold Nanorods. *J. Phys. Chem. B* **2001**, *105*, 4065–4067.
24. Murphy, C. J.; Jana, N. R. Controlling the Aspect Ratio of Inorganic Nanorods and Nanowires. *Adv. Mater.* **2002**, *14*, 80–82.
25. Nikoobakht, B.; El-Sayed, M. A. Evidence for Bilayer Assembly of Cationic Surfactants on the Surface of Gold Nanorods. *Langmuir* **2000**, *17*, 6368–6374.
26. Gao, J. X.; Bender, C. M.; Murphy, C. J. Dependence of the Gold Nanorod Aspect Ratio on the Nature of the Directing Surfactant in Aqueous Solution. *Langmuir* **2003**, *19*, 9065–9070.
27. Liao, H.; Hafner, J. H. Gold Nanorod Bioconjugates. *Chem. Mater.* **2005**, *17*, 4636–4641.
28. Gole, A.; Murphy, C. J. Polyelectrolyte-Coated Gold Nanorods: Synthesis, Characterization and Immobilization. *Chem. Mater.* **2005**, *17*, 1325–1330.
29. Orendorff, C. J.; Murphy, C. J. Quantitation of Metal Content in the Silver-Assisted Growth of Gold Nanorods. *J. Phys. Chem. B* **2006**, *110*, 3990–3994.
30. Hubert, F.; Testard, F.; Spalla, O. Cetyltrimethylammonium Bromide Silver Bromide Complex as the Capping Agent of Gold Nanorods. *Langmuir* **2008**, *24*, 9219–9222.
31. Kreke, P. J.; Magid, L. J.; Gee, J. C. ^{1}H and ^{13}C NMR Studies of Mixed Counterion, Cetyltrimethylammonium Bromide/Cetyltrimethylammonium Dichlorobenzoate, Surfactant Solutions: The Intercalation of Aromatic Counterions. *Langmuir* **1996**, *12*, 699–705.
32. Li, K.-L.; Tihal, C. A.; Guo, M.; Stark, R. E. Multinuclear and Magic-Angle-Spinning NMR Investigations of Molecular Organization in Phospholipid-Triglyceride Aqueous Dispersions. *Biochemistry* **1993**, *32*, 9926–9935.
33. Cruciana, O.; Mannina, L.; Sobolev, A. P.; Cametti, C.; Serge, A. An Improved NMR Study of Liposomes Using 1-Palmitoyl-2-oleoyl-*sn*-glycero-3-phospatidylcholine as Model. *Molecules* **2006**, *11*, 334–344.
34. Sui, Z. M.; Chen, X.; Wang, L. Y.; Xu, L. M.; Zhuang, W. C.; Chai, Y. C.; Yang, C. J. Capping Effect of CTAB on Positively Charged Ag Nanoparticles. *Physica E* **2006**, *33*, 308–314.
35. Terrill, R. H.; Postlethwaite, T. A.; Chen, C.-h.; Poon, C.-D.; Terzis, A.; Chen, A.; Hutchison, J. E.; Clark, M. R.; Wignall, G.; Londono, J. D.; *et al.* Monolayers in Three Dimensions: NMR, SAXS, Thermal, and Electron Hopping Studies of Alkanethiol Stabilized Gold Clusters. *J. Am. Chem. Soc.* **1995**, *117*, 12537–12548.
36. Kumar, A.; Mandal, S.; Selvakannan, P. R.; Pashicha, R.; Mandale, A. B.; Sastry, M. Investigation into the Interaction between Surface-Bound Alkylamines and Gold Nanoparticles. *Langmuir* **2003**, *19*, 6277–6282.
37. Leff, D. V.; Brandt, L.; Heath, J. R. Synthesis and Characterization of Hydrophobic, Organically-Soluble Gold Nanocrystals Functionalized with Primary Amines. *Langmuir* **1996**, *12*, 4723–4730.
38. Porta, F.; Krpetic, Z.; Prati, L.; Gaiassi, A.; Scari, G. Gold-Ligand Interaction Studies of Water-Soluble Aminoalcohol Capped Gold Nanoparticles by NMR. *Langmuir* **2008**, *24*, 7061–7064.
39. Yang, C.; Chen, X.; Sui, Z.; Wang, L. Molecular Dynamics Simulation of a Positively Charged Silver Nanoparticle Capped by Cetyltrimethylammonium Cations. *Colloids Surf., A* **2006**, *274*, 219–222.
40. Cui, X.; Mao, S.; Liu, M.; Yuan, H.; Du, Y. Mechanism of Surfactant Micelle Formation. *Langmuir* **2008**, *24*, 10771–10775.
41. Howarth, V. A.; Petty, M. C.; Ancelin, H.; Yarwood, J. Structural Characterization of Phospholipid Langmuir−Blodgett Multilayers Containing Valinomycin. *Vib. Spectrosc.* **1990**, *1*, 29–33.
42. Sarag, L. T. M.; Okamura, E.; Umemura, J.; Takenaka, T. Fourier Transform Infrared-Attenuated Total Reflection Spectroscopy of Hydration of Dimyristoylphosphatidylcholine Multibilayers. *Biochim. Biophys. Acta* **1998**, *946*, 417–423.
43. Hubner, W.; Mantsch, H. H. Orientation of specifically $^{13}C{=}O$ Labeled Phosphatidylcholine Multilayers from Polarized Attenuated Total Reflection FT-IR Spectroscopy. *Biophys. J.* **1991**, *59*, 1261–1272.
44. Lin-Vien, D.; Colthup, N. B.; Fateley, W. G.; Grasselli, J. G. *The Handbook of Infrared and Raman Characteristic Frequencies of Organic Molecules*; Academic Press: New York, 1991.
45. Jaing, C.; Gamarnik, A.; Tripp, C. P. Identification of Lipid Aggregate Structures on TiO_2 Surface Using Headgroup IR Bands. *J. Phys. Chem. B* **2005**, *109*, 4539–4544.
46. Zawisza, I.; Nullmeier, M.; Pust, S. E.; Boukherroub, R.; Szunerits, S.; Wittstock, G. Application of Thin Titanium/Titanium Oxide Layers Deposited on Gold for Infrared Reflection Absorption Spectroscopy: Structural Studies of Lipid Bilayers. *Langmuir* **2008**, *24*, 7378–7387.
47. Li, H.; Tripp, C. P. Spectroscopic Identification and Dynamics of Adsorbed Cetyltrimethylammonium Bromide Structures on TiO_2 Surfaces. *Langmuir* **2002**, *18*, 9441–9446.
48. Zawisza, I.; Bin, X.; Lipkowski, J. Potential-Driven Structural Changes in Langmuir−Blodgett DMPC Bilayers Determined by *In Situ* Spectroelectrochemical PM IRRAS. *Langmuir* **2007**, *23*, 5180–5194.
49. Fringeli, U. P. Structure of Lipids and Proteins Studied by Attenuated Total Reflection (ATR) Infrared Spectroscopy 2. Oreinted Layters of a Homologous Series—Phosphatidylethanolamine to Phasphatidylcholine. *Z. Naturforsch. C* **1977**, *32*, 20–45.
50. Moncelli, M. R.; Becucci, L.; Guidelli, R. The Intrinsic pK_a Values for Phosphatidylcholine, Phosphatidylethanolamine, and Phosphatidylserine in Monolayers Deposited on Mercury Electrodes. *Biophys. J.* **1994**, *66*, 1969–1980.
51. Marsh, D. *CRC Handbook of Lipid Bilayers*; CRC Press: Boca Raton, FL, 1990.
52. Creager, S. E.; Clarke, J. Contact-Angle Titrations of Mixed ω-Mercaptoalkanoic Acid/Alkanethiol Monolayers on Gold. Reactive *vs* Nonreactive Spreading, and Chain Length Effects on Surface pK_a Values. *Langmuir* **1994**, *10*, 3675–3683.
53. White, H. S.; Peterson, J. D.; Cui, Q.; Stevenson, K. J. Voltammetric Measurement of Interfacial Acid/Base Reactions. *J. Phys. Chem. B* **1998**, *102*, 2930–2934.
54. Vermeer, A. W. P.; Leermarkers, F. A. M.; Koopal, L. K. Adsorption of Weak Polyelectrolytes on Surfaces with a Variable Charge. Self-Consistent-Field Calculations. *Langmuir* **1997**, *13*, 4413–4421.
55. Hu, K.; Bard, A. J. Use of Atomic Force Microscopy for the Study of Surface Acid−Base Properties of Carboxylic Acid-Terminated Self-Assembled Monolayers. *Langmuir* **1997**, *13*, 5114–5119.
56. Thomas, C. F.; Luisi, P. L. RNA Selectively Interacts with Vesicles Depending on Their Size. *J. Phys. Chem. B* **2005**, *109*, 14544–14550.

57. El-Sayed, M. A. Some Interesting Properties of Metals Confined in Time and Nanometer Space of Different Shapes. *Acc. Chem. Res.* **2001**, *34*, 257–264.
58. Mock, J. J.; Smith, D. R.; Schultz, S. Local Refractive Index Dependence of Plasmon Resonance Spectra from Individual Nanoparticles. *Nano Lett.* **2003**, *3*, 485–491.
59. Su, K.−H.; Wei, Q.−H.; Zhang, X.; Mock, J. J.; Smith, D. R.; Schultz, S. Interparticle Coupling Effects on Plasmon Resonances of Nanogold Particles. *Nano Lett.* **2003**, *3*, 1087–1091.
60. Johnson, C. J.; Dujardin, E.; Davis, S. A.; Murphy, C. J.; Mann, S. Growth and Form of Gold Nanorods Prepared by Seed-Mediated, Surfactant-Directed Synthesis. *J. Mater. Chem.* **2002**, *12*, 1765–1770.
61. Jana, N. R.; Gearheart, L.; Obare, S. O.; Murphy, C. J. Anisotropic Chemical Reactivity of Gold Spheroids and Nanorods. *Langmuir* **2002**, *18*, 922–927.
62. Sau, T. K.; Murphy, C. J. Self-Assembly Patterns Formed upon Solvent Evaporation of Aqueous Cetyltrimethylammonium Bromide-Coated Gold Nanoparticles of Various Shapes. *Langmuir* **2005**, *21*, 2923–2929.
63. Zhang, Z.; Glotzer, S. C. Self-Assembly of Patchy Particles. *Nano Lett.* **2004**, *4*, 1407–1413.